SIN-CHN
SCIENTIFIC PRESS PTE.LTD.

Molecular & Cellular Biomechanics 2024, 21, 174.
https://doi.org/10.62617/mcb.v21.174

Article

Utilization of NIR photosensitive π-conjugated materials in sports using near infrared spectroscopy imaging: Real-time measurement of muscle oxygenation levels

Haiguang Hu, Na Zhou*

College of General Education, Guangxi Vocational University of Agriculture, Nanning 530007, China
*** Corresponding author:** Na Zhou, zhouna810609@163.com

CITATION

Hu H, Zhou N. Utilization of NIR photosensitive π-conjugated materials in sports using near infrared spectroscopy imaging: Real-time measurement of muscle oxygenation levels. Molecular & Cellular Biomechanics. 2024; 21: 174. https://doi.org/10.62617/mcb.v21.174

ARTICLE INFO

Received: 29 May 2024
Accepted: 24 June 2024
Available online: 2 August 2024

Abstract: The measurement of muscle oxygenation levels by near infrared spectroscopy imaging technology is hindered by light scattering and absorption in tissues. This leads to a limited measurement range and necessitates a significant amount of time for optical signal acquisition. Therefore, this article used photosensitive π-conjugated materials for measurement optimization in near infrared spectroscopy imaging technology. Firstly, photosensitive π-conjugated materials were applied to near infrared spectrometers for spectral measurements. Secondly, the elimination of uninformative variables and the ratio of regression coefficients to spectral residuals were used for wavelength screening. Subsequently, the spectral data was preprocessed, and principal component analysis was used for quantitative correction. Finally, the effectiveness of near infrared spectroscopy imaging technology optimized using photosensitive π-conjugated materials was verified through experiments. In terms of measurement range, the near infrared spectrometer optimized using photosensitive π-conjugated materials expanded the measurement range by 42.7%; in terms of optical signal acquisition time and measurement accuracy, the acquisition time of near infrared spectrometers optimized with photosensitive π-conjugated materials was shorter than that of near infrared spectrometers optimized without photosensitive π-conjugated materials. In terms of measurement accuracy, the near infrared spectrometer optimized using photosensitive π-conjugated materials had higher accuracy, both exceeding 98%. The use of photosensitive π-conjugated materials in near infrared spectral imaging analysis had good monitoring effects, and could quickly, accurately, and comprehensively measure muscle oxygenation levels, making it very suitable for application in sports.

Keywords: muscle oxygenation levels; near infrared spectroscopy imaging; photosensitive π-conjugated materials; wavelength screening; spectral pretreatment

1. Introduction

Muscle fatigue is a common condition in sports activities. By observing changes in muscle oxygenation levels, the fatigue level of muscles during sports can be evaluated. When muscles feel tired, the use and supply of oxygen may be restricted, resulting in a decrease in muscle oxygenation levels. Traditional near infrared spectroscopy imaging technology is susceptible to factors such as blood flow and tissue scattering when measuring muscle oxygenation levels, thereby reducing detection accuracy. The muscle tissue structure and blood flow situation may vary among different populations, which limits the comprehensive evaluation of the oxygenation level of the entire muscle using near infrared spectroscopy technology. It can only measure the surface of the muscle and cannot obtain the oxygenation level of deep muscle tissue. Therefore, based on traditional near infrared spectroscopy imaging

technology, photosensitive π-conjugated materials are used to optimize and monitor changes in muscle oxygenation levels. When this material comes into contact with muscles or is placed on the skin, it can perceive changes in the near infrared light reflection of muscle tissue and convert these changes into corresponding signals. In addition, it can also detect the dynamic changes in intramuscular oxygen concentration and monitor the metabolic process and oxygen supply status of muscles in real-time. These are of great importance for in-depth research in sports physiology, real-time monitoring of sports training, and comprehensive evaluation of the rehabilitation stage.

Currently, research on monitoring muscle oxygenation levels is receiving increasing attention. Measuring muscle oxygen levels can evaluate muscle oxygen supply capacity, fatigue during sports, and recovery effectiveness [1,2]. This helps to arrange sports training more reasonably, optimize rehabilitation plans, and improve sports performance and rehabilitation effectiveness [3,4]. Jiang and Dai [5] summarized the basic theory of muscle oxygen measurement, as well as the research progress in functional state evaluation, assessment of aerobic metabolic capacity, load intensity monitoring, sports effectiveness and rehabilitation ability judgment through literature review. Li et al. [6] and Duan and Li [7] used neuromuscular electrical stimulation (NMES) on the basis of monitoring muscle oxygen levels to perform lower limb resistance training on hemiplegic patients after stroke, and verified the clinical efficacy of the treatment through experiments. Under the guidance of muscle oxygen level monitoring, Xiao et al. [8] analyzed the body composition and muscle oxygen saturation of obese college students after 12 weeks of fat oxidation intensity sports, and provided scientific reference for weight loss and aerobic capacity evaluation of obese college students based on the impact of relevant situations. Gao et al. [9] monitored the muscle oxygen content of both sports and non-sports, and observed the response of muscle oxygen content and vascular elasticity to load sports. The experiment found that regular sports can improve the recovery speed of skeletal muscle oxygen content. In short, monitoring can better guide rehabilitation training and promote health management. By monitoring changes in muscle oxygenation levels, problems in the body can be identified in a timely manner, and corresponding measures can be taken to prevent the occurrence of diseases.

Near infrared spectroscopy, as a fast, non-destructive, and diverse analytical method, has been widely applied in various fields [10,11]. The development and application of near infrared spectroscopy further expands its new research fields and application scope [12,13]. Hu et al. [14] used 119 rubber trees as the research object to quantitatively analyze leaf nitrogen using near infrared spectroscopy, and constructed a high-precision leaf nitrogen content prediction model to achieve rapid and accurate measurement of nitrogen content. Zhu [15] used a combination of near infrared spectroscopy and partial least squares method to achieve rapid detection of threonine and valine in buckwheat leaves in response to the problems in the breeding and production process of buckwheat varieties. Liang et al. [16] used near infrared spectroscopy technology to measure the basic density of pulp fibers, achieving real-time monitoring of pulp raw material performance, and providing theoretical basis for the design and optimization of pulp processing processes. Hao et al. [17] used near infrared spectroscopy to characterize the quality of tobacco leaf formula design, and combined partial least squares method to construct a near infrared spectral model of

tobacco leaves, achieving prediction of tobacco leaf quality. Ge et al. [18] used near infrared spectroscopy technology as the main research method, and used Unscrambler software and partial least squares method to establish a near infrared spectroscopy prediction model for the fat content of Xanthoceras sorbifolia, achieving non-destructive and rapid detection of Xanthoceras sorbifolia fat content. The research of the above scholars reflects the excellent performance of near infrared spectroscopy monitoring. Therefore, combining near infrared spectroscopy imaging analysis with photosensitive π-conjugated materials to determine muscle oxygenation levels and obtain objective data on muscle fatigue status is feasible.

In summary, this article aimed to study the use of NIR (near infrared) photosensitive π-conjugated materials to measure muscle oxygenation levels. The research first briefly explained the imaging principle of near infrared spectroscopy, and then applied photosensitive π-conjugated materials in near infrared spectrometers. Next, the measurement of near infrared spectroscopy was analyzed, mainly considering three aspects: wavelength screening, spectral preprocessing, and calibration. Wavelength screening uses the elimination of uninformative variables and the ratio of regression coefficients to spectral residuals to enhance the robustness of spectral measurements. Spectral preprocessing uses the Savitzky-Golay smoothing method in smoothing, variable standardization, and multivariate scattering correction to reduce interference factors in the measurement process and highlight valuable information. The correction mainly uses principal component analysis to eliminate the impact. Finally, with 15 athletes as the research subjects, the muscle oxygenation level measurement method used in this article was experimentally analyzed to compare the near infrared spectroscopy measurement effects before and after optimization.

2. Near infrared spectral imaging measurement method

2.1. Near infrared spectral imaging

Near infrared (NIR, wavelength range of 700–2500 nm) has high tissue penetration ability, making NIR spectroscopy imaging possible [19]. When NIR light irradiates biological tissues, a portion of the light is absorbed, while the remaining portion is reflected or transmitted [20,21]. This reflected or transmitted spectrum can reflect the internal structure of tissues, including the oxygenation state of muscles.

Near infrared spectroscopy analysis, as a non-invasive technical means, is used to measure the oxygenation level content in muscle tissue. The near infrared spectrometer consists of a portable light source, an optical detector, and a computer, which utilizes the inherent characteristics of biological samples themselves. Due to the relatively high concentration of blood in the muscles, using near infrared spectroscopy for detection has become very important.

Near infrared spectroscopy technology is based on the absorption and scattering properties of near infrared light within tissues. Detecting the aerobic content in human muscles accurately determines the level of muscle oxygen by measuring the ratio of oxygenated hemoglobin to deoxyhemoglobin within the tissue. When conducting measurements, a near infrared light source shines through the skin into muscle tissue. Due to the strength of elasticity of muscles, they can reflect light from within tissues back to the outside of the human body. After being absorbed and scattered by tissues,

light is captured and analyzed by a near infrared spectrometer. This device is used to detect human muscles and obtain their absorption spectra. By analyzing the absorption characteristics of light, the content of oxygenated hemoglobin and deoxyhemoglobin in tissues can be calculated to determine the oxygenation level of muscles.

NIR photosensitive π-conjugated materials are a special substance with π-conjugated structures that can strongly absorb and emit NIR light. These materials undergo photochemical reactions when exposed to specific wavelengths of NIR light, thereby altering their fluorescence properties. Detecting these changes enables us to infer the physiological parameters of the tissue.

The operation of applying photosensitive π-conjugated materials to near infrared spectrometers is as follows:

Step 1: Preparing photosensitive π-conjugated materials

Indocyanine dyes in photosensitive π-conjugated materials are selected to ensure that the infrared absorption range of the material matches the working wavelength range of the near infrared spectrometer.

Step 2: Preparation of sensors

Photosensitive π-conjugated materials are prepared as sensors. The material is dissolved in an appropriate solvent and coated on a polymer substrate through immersion coating, spraying, and deposition methods.

Step 3: Connecting the sensor

The prepared photosensitive π-conjugated material sensor is connected to the adapter of the near infrared spectrometer to ensure good circuit connection between the sensor and the instrument.

Step 4: Starting the near infrared spectrometer

The near infrared spectrometer is activated for preheating and calibration.

Step 5: Performing spectral measurement

The sample to be measured is placed below the sensor to ensure that near infrared light illuminates the photosensitive π-conjugated material.

Step 6: Recording spectral data

The near infrared spectrometer records the absorption and scattering of light by photosensitive π-conjugated materials, and generates spectral data. Spectral data is viewed and saved through the instrument's display screen, computer software, and connected mobile devices.

Performance tests were conducted for the NIR spectrometer equipment used, as shown in **Table 1** below.

Table 1. Performance tests of the equipment.

	Test item	**Test parameters**	**Test results**
1	Spectral accuracy	Perform spectral measurements using standard calibration samples	Measurement results within acceptable range
2	Spectral stability	Perform consecutive spectral measurements, record changes in absorbance	Absorbance changes within the specified threshold
3	Reproducibility	Perform multiple measurements on the same sample, record differences in absorbance	Absorbance differences within acceptable range
4	Environmental adaptability	Perform spectral measurements under different temperature and humidity conditions	Consistent measurement results under different conditions

Table 1. (*Continued*).

	Test item	Test parameters	Test results
5	Fault detection and recovery	Simulate device faults such as sensor disconnection or circuit connection issues	Device detects faults promptly and performs necessary recovery actions
6	Long-term stability	Continuous operation of the device for spectral measurements, record changes in device performance over time	Device performance remains stable during the test period without significant degradation or drift
7	Durability	Conduct long-term continuous operation testing, record device operation and faults	Device operates stably throughout the test period without major faults

The tests of each item in **Table 1** have proved that the equipment used in this paper has various functional standards, good performance and durability.

2.2. Application in sports science

The application of near infrared spectroscopy in sports science is shown in **Figure 1**.

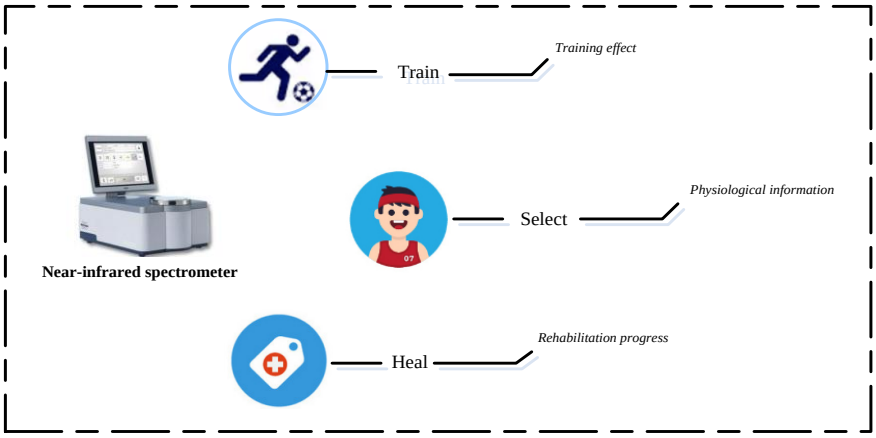

Figure 1. Application of near infrared spectroscopy.

Figure 1 shows the application of near infrared spectroscopy in three aspects of sports science:

1) Athlete training

Through near infrared spectroscopy imaging, the training effectiveness of athletes is monitored in real-time, including muscle fatigue and recovery time [22], which helps coaches develop more reasonable training plans and improve the training effectiveness of athletes.

2) Athlete selection

In competitive sports, accurate muscle oxygenation measurements can help select athletes with potential. Near infrared spectroscopy imaging technology can provide comprehensive physiological information of athletes, which is helpful for selection decision-making.

3) Rehabilitation treatment

For athletes who are injured or sick, near infrared spectroscopy imaging technology can monitor their rehabilitation progress. By monitoring muscle oxygenation levels in real-time, rehabilitation plans can be formulated more effectively.

3. Near infrared spectroscopy imaging method

3.1. Wavelength screening method

Combine heart rate monitoring and near-infrared spectroscopy to more comprehensively assess exercise intensity and cardiopulmonary function and optimize training programs. Heart rate monitoring is responsible for providing a direct indicator of heart function, and NIR spectroscopy provides oxygen supply and demand status of local muscles. Through heart rate monitoring, the heart rate (reflecting the number of heart beats per minute), the maximum heart rate (used to develop training plans), and the heart rate variability (reflecting changes in the time interval between heart beats) are obtained in real time.

The muscle component content contains multiple molecules and groups (as shown in **Figure 2**), and some groups correspond to weak absorption and reflection light intensity, which makes it impossible to obtain spectral data of each component content from all measured spectral information. There is also mutual interference between muscle component contents, resulting in poor predictive performance and robustness of the quantitative correction model for the measured spectral data. Therefore, it is necessary to select an appropriate wavelength for near infrared spectral analysis based on the obtained spectral data.

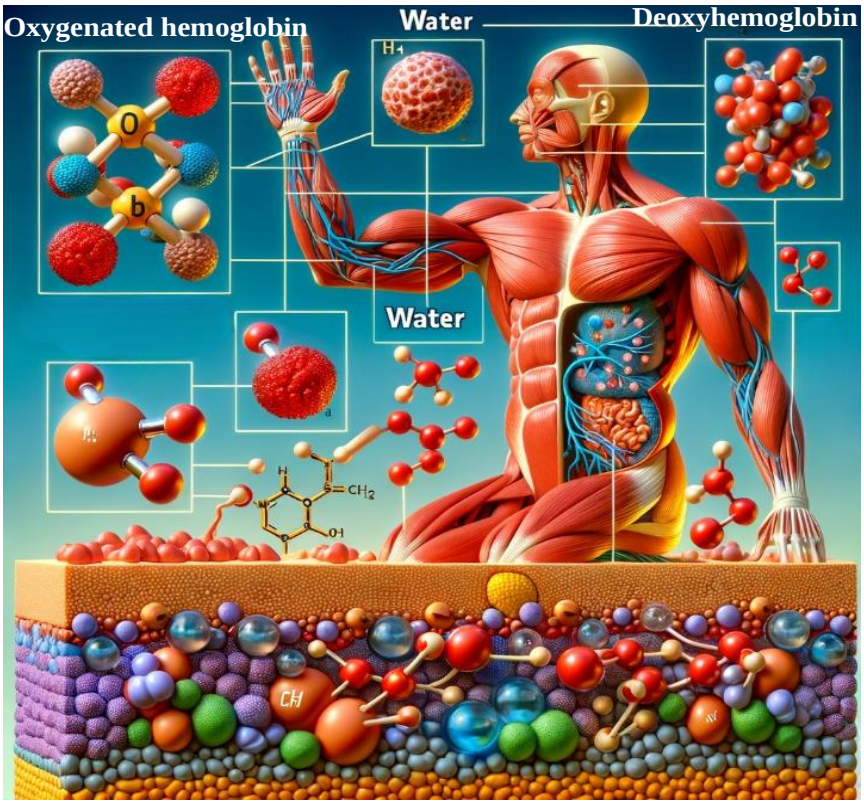

Figure 2. Muscle composition content.

Figure 2 shows the various components of muscle tissue, including oxygenated hemoglobin, deoxygenated hemoglobin, and water.

The wavelength selection methods selected in this article include: uninformative variable elimination method, ratio of regression coefficients to spectral residuals.

1) Uninformative variable elimination (UVE)

The uninformed variable elimination method is a statistical based feature selection method used in multivariate spectral analysis to remove features (uninformed variables) that are not related to the predicted variables [23]. By utilizing the correlation degree or amount of information between spectral features and the variables to be measured, the importance of information is evaluated, and features without information variables are eliminated according to pre-set thresholds or rankings.

The uninformative variable elimination method is also a wavelength screening method, and its principle is based on the partial least squares regression coefficient a. On this basis, the Leave-One-Out Cross-Validation (LOO-CV) algorithm is used to analyze the stability of each variable, and then wavelength screening is performed based on the size of the stability. The regression model with X as the variable and Y as the target value is as follows:

$$Y = X\delta + a_o \tag{1}$$

By leaving a cross validation algorithm, a regression coefficient matrix $\delta = [\delta 1, \delta 2, ..., \delta n]$ can be obtained. The stability definition expression for each variable is as follows:

$$W_i = mean(\delta_i)/std(\delta_i) \tag{2}$$

Among them, $mean(\delta_i)$ refers to the average value of δ_i, and $std(\delta_i)$ refers to the standard deviation of δ_i. According to Equation (2), it is evident that when the average value is large and the standard deviation is small, W_i is larger. This indicates that the corresponding variables are relatively stable during cross validation. On the contrary, it indicates that the corresponding variable is unstable.

In the process of using the uninformed variable elimination method for calculation, it is necessary to determine a standard for the size of stability by artificially adding the same amount of random noise *Z* to *X*. If a variable with less stability than random noise is considered an uninformative variable, it should be removed from the model. In actual calculations, the numerical value of cutoff is calculated as follows:

$$cutoff = K \times max(abs(W_{noise})) \tag{3}$$

Among them, $cutoff$ refers to a predetermined threshold, and K refers to controllable parameters.

2) Wavelength optimization method based on the ratio of regression coefficients to spectral residuals

The wavelength optimization method based on the ratio of regression coefficients to spectral residuals is a feature selection method based on regression models. This method evaluates the predictive ability of different spectral characteristics on target variables by constructing a regression model. On this basis, the regression coefficients of each feature and the ratio of spectral residuals are sorted, and the feature with the highest ratio is selected as the main feature [24].

The wavelength screening expression for the wavelength selection method based on the ratio of regression coefficients to spectral residuals is:

$$V_i = \left| \frac{\widehat{h_\iota}}{\sqrt[4]{\hat{C}_{c_i}}} \right| \tag{4}$$

The variable definition of Equation (4) is shown in **Table 2**.

Table 2. Explanation of wavelength screening expression variables.

Sequence	Variable	Meaning
1	V_i	Ratio of the regression coefficient to the spectral residual for the *i*th wavelength
2	$\widehat{h_1}$	The regression coefficient of the *i* wavelength is calculated
3	$\hat{C}_{c_i}$	Spectral residual at the *I*-wavelength

3.2. Spectral preprocessing

In the process of collecting spectral data of muscle oxygenation level samples, due to various factors such as environmental conditions, instrument equipment, human intervention, and the characteristics of the samples themselves, spectral signals not only cover the physical and chemical properties of the tested muscles, but also contain a large amount of scattered light, noise, and background information. Although near infrared spectrometers use multiple average acquisition methods for spectral data collection to maximize the signal-to-noise ratio of the signal, spectral noise and interference are still inevitable, and these factors have a significant impact on the analysis of spectral signals and the construction of the final relationship model.

In addition, due to the influence of external environmental factors, there is often a certain degree of non-uniformity in the measured muscle oxygenation level, resulting in errors or even errors in the measurement results. Therefore, in the process of preprocessing the collected raw spectra, it is crucial to strive to exclude all possible interference factors from the spectral data to maximize the highlighting of valuable information in the near infrared spectrum. This operation is crucial.

The common preprocessing methods for near infrared spectroscopy mainly include data enhancement conversion, smoothing processing, derivative operation, variable standardization processing, and multivariate scattering correction [25].

This article mainly selects the Savitzky-Golay smoothing method in smoothing processing, standard normal variate, and multivariate scattering correction for near infrared spectral data preprocessing.

1) Savitzky-Golay smoothing method

We selected the Savitzky-Golay smoothing method for preprocessing near-infrared spectral data, as illustrated in **Figure 3**. Savitzky-Golay smoothing method is a commonly used near infrared spectral data smoothing method, which mainly estimates the smoothing value of data points through polynomial fitting [26,27].

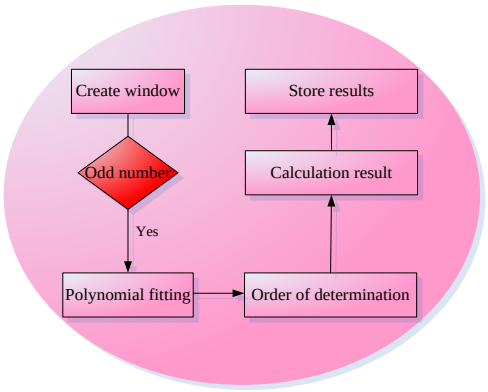

Figure 3. Processing operation of Savitzky-Golay smoothing method.

Figure 3 shows the specific operation of Savitzky-Golay smoothing method for preprocessing near infrared spectral data: the first step is to create a window and determine the parity of the window size. If the window size is odd (the window size must be odd), the next step is polynomial fitting.

The second step is to slide the window from the starting position of the dataset to the ending position, and use the least squares method for polynomial fitting. The polynomial expression is:

$$F(x) = N_0 + N_1 * x + N_2 * x\text{^}2 + \cdots + N_m * x\text{^}m \quad (5)$$

$F(x)$ refers to a polynomial function, x refers to the independent variable, N_0, N_1, ..., N_m refers to the coefficients to be fitted.

In order to minimize the error of polynomial fitting, the expression of the error function is:

$$E(N_0, N_1, N_2, \ldots\ldots, N_m) = \sum (g_i - F(x_i))\text{^}2 \quad (6)$$

In the expression, g_i refers to the observed value corresponding to the data, and x_i refers to the value of the independent variable.

The third step is to determine the order of polynomial fitting as 1; the fourth step is to use polynomial fitting to calculate the smoothing results of the window; the fifth step is to store the calculated results.

2) Standard normal variable (SNV)

The basic law of absorbance value is Lambert-Beer Law, which is also the basis for quantitative analysis of spectra [28,29]. The expression for the absorbance value is as follows:

$$A_\gamma = -log\, 10L = ahn \quad (7)$$

The definition of expression variables is shown in **Table 3**.

Table 3. Explanation of variables in the expression of absorbance values.

Sequence	Variable	Meaning
1	A_γ	Absorbance at wavelength γ
2	L	Light transmittance
3	a	Absorption coefficient
4	h	Absorption layer thickness
5	n	The concentration of light-absorbing substances

Preprocessing near infrared spectral data based on Lambert-Beer Law can more accurately establish the correspondence between A and n, and extract feature information from different types of samples, thus achieving the goal of quantitative and qualitative analysis of complex systems.

Standard normal variate is achieved by converting the absorbance values of each wavelength to ensure that the results follow a normal distribution [30]. The calculation formula is as follows:

$$P_{SNV} = \frac{P - \bar{P}}{\sqrt{\frac{\sum_{i=1}^{\gamma}(P_i - \bar{P})}{\gamma - 1}}} \tag{8}$$

The definition of formula variables is shown in **Table 4**.

Table 4. Definition of formula variables.

Sequence	Variable	Meaning
1	P	Primary spectrum
2	$\overline{P}$	The average absorbance value of each wavelength point
3	γ	Wavelength number

The operation process of variable standardization enables the original spectral data to achieve standard normalization, resulting in standard deviation and average error of 1 and 0, respectively, for the spectral data.

3) Multivariate scattering correction

Light undergoes multiple scattering within the muscle oxygenation level measurement sample, making the propagation path of light longer, thereby affecting the intensity and spectral morphology of light. This is called multivariate scattering [31,32].

Multiple scattering correction is mainly used for preprocessing depolarized spectral data to reduce the adverse impact of multiple scattering on spectral measurement accuracy [33,34].

The processing formulas for multivariate scattering correction are as follows:

$$\bar{S} = \frac{1}{j}\sum_{i=1}^{j} P_i \tag{9}$$

$$P_i = f_i\bar{S} + y_i \tag{10}$$

$$P_i, MSC = \frac{P_i - y_i}{f_i} \tag{11}$$

The meanings of variables in Equations (9)–(11) for multivariate scattering correction processing are shown in **Table 5**.

Table 5. Interpretation of variables in the multivariate scattering correction formulas.

Sequence	Variable	Meaning
1	$\bar{S}$	Mean spectrum
2	i	Sample label
3	P_i	Original spectrum of sample *i*
4	f_i	Spectral drift
5	P_i, MSC	Data processed by standard normal variate trans-formation

Standard normal variable transformation is the process of subtracting the average of spectral data from each spectral data and dividing it by the standard deviation of the spectral data:

$$P_i, SNV = \frac{P_i - \bar{S}}{\varepsilon} \tag{12}$$

Among them, ε is the standard deviation of near infrared spectral data.

3.3. Spectral correction

Due to the large and complex composition in muscle tissue, the content spectra of muscle oxygenation levels obtained by near infrared spectroscopy have mutual influence, so principal component analysis is chosen for spectral correction.

Spectral correction is the correction of the measurement results of muscle oxygenation levels. In practical work, due to the large amount of scattered information such as diffraction, absorption, and reflection contained in the spectral measurement results, this information cannot be fully extracted. In order to improve the accuracy and reliability of measurement results, it is necessary to calibrate these spectral values.

Principal component analysis is often used for data dimensionality reduction and feature extraction [35,36]. During the quantitative correction process, principal component analysis is used to model the measurement samples through linear regression and correct them. The correction formula is as follows:

$$G_{m\times p} = S_{m\times d} V_{d\times p} + O_A \tag{13}$$

The variable definition of the correction formula is shown in **Table 6**.

Table 6. Interpretation of correction formula variables.

Sequence	Variable	Meaning
1	$G_{m\times p}$	Spectral matrix
2	$S_{m\times d}$	Spectral score matrix
3	$V_{d\times p}$	Principal component matrix
4	O_A	Predicted spectral residuals

Next, compare the cost-effectiveness of the existing Fourier transform technique (J1) applied to the NIR spectrometer with the new technique (J2) applied to the NIR spectrometer using photosensitive pi-conjugated materials, as shown in **Table 7** below.

Table 7. Cost-effectiveness between different technologies.

Item	J1	J2	Cost savings/benefits
Material cost	$200 per experiment	$300 per experiment	Reduce experiment times, long-term savings of 20%
Equipment cost	$50,000	$75,000	Maintenance cost reduced by 30%
Laboratory operating cost	$10,000 per month	$7000 per month	Monthly savings of 30%
Data analysis and software cost	$5000 per year	$8000 per year	Analysis time reduced by 50%
Personnel training and technical support	$3000 per year	$5000 per year	Support needs reduced by 40%
Research and development cost	$30,000 per year	$50,000 per year	Return rate increased by 50%
Publication and patent application cost	$2000 per paper/patent	$3000 per paper/patent	Recognition increased by 30%
Number of experiments per year	100 times	80 times	Annual experiment times reduced by 20%
Measurement time per experiment	60 minutes	40 minutes	Measurement time reduced by 33%

As can be seen from **Table 7**, the new technology of using photosensitive pi-conjugated materials for NIR spectroscopy has significant advantages in terms of economic advantages and potential savings. Although the initial cost is high, it has significant advantages in experimental efficiency, data processing and long-term research and development, which can bring long-term economic and academic benefits.

4. Spectral measurement experiment

4.1. Experimental setup

A near infrared spectrometer without photosensitive π-conjugated materials and a near infrared spectrometer with photosensitive π-conjugated materials used in this article were selected for experimental testing. These two instruments were named T1 and T2, respectively. Fifteen athletes were randomly selected to use these two instruments to measure muscle oxygenation levels separately. The parameter settings for these two instruments were: the spectrum was set to the average of 128 consecutive scans; the wavenumber range was set to 5000–11000 cm^{-1}; the resolution was set to 3 cm^{-1}. Among them, each spectrum contains 3245 data points, and the data recording format is represented by Log 1/R.

Before the experiment, the two instruments were used to make several continuous spectral measurements of the same specimen, and the change of absorption intensity was recorded after each measurement. The absorption intensity values in the same wave number range were selected for comparison, and the standard deviation and mean value of the absorption intensity were calculated. It was found that the difference of the absorption intensity was within the acceptable range, indicating that the measurement results of the two instruments had a good consistency.

Before the start of the experiment, the selected athletes were given detailed training and instructions to fully understand the purpose, process and related requirements of the measurement. Explain the operation process and precautions of the instrument to ensure that athletes understand and master the measurement technique. At the same time, before the formal measurement, a period of adaptive training. Let the athletes use the measuring equipment and perform simulated

measurement operations to familiarize themselves with the measurement process, the use of the instrument and the acquisition of data. Gradually increase the difficulty and complexity of training to improve the adaptability of athletes to measurement technology.

Comprehensive safety assessment before application of photosensitive PI-conjugated materials to human subjects, 1) Initial assessment: chemical composition analysis (identification of potential irritants), in vitro cell testing (detection of toxicity to skin cells).

Skin allergen testing (screening for sensitization potential). 2) Preclinical evaluation: acute and chronic skin irritation tests (observation of long- and short-term skin reactions), phototoxicity tests (detection of toxicity under light conditions), 3) Clinical studies: set up different levels of phase I (small healthy subjects), phase II (further evaluation in the target population), and phase III trials (large-scale validation of safety and efficacy). 4) Monitoring and reporting: long-term safety monitoring and continuous data analysis.

4.2. Measurement range

The larger the measurement range of the near infrared spectrometer, the more chemical components or molecular characteristics of muscle oxygenation levels detected. At the same time, it can also provide more spectral data, which can comprehensively analyze the structure and properties of athlete muscle oxygenation levels. The test results are shown in **Figure 4**.

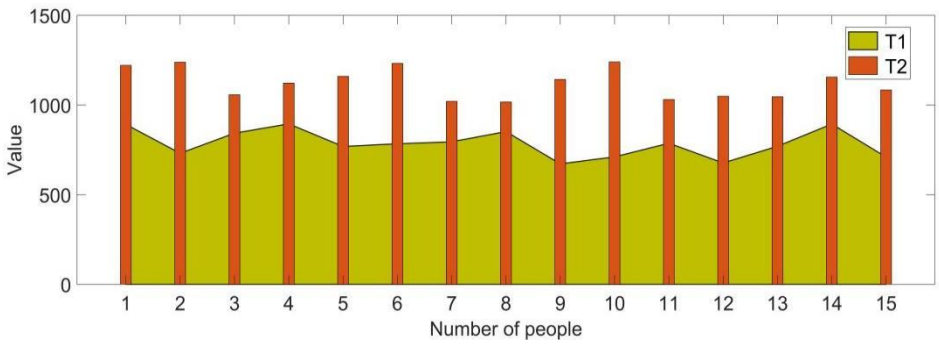

Figure 4. Measurement range of T1 and T2 in nanometers.

Figure 4 shows the measurement range of T1 and T2 for these 15 athletes very well. Among them, T1 had a measurement range of less than 1000 nanometers, while T2 had a measurement range of over 1000 nanometers. It is evident that near infrared spectrometers using photosensitive π-conjugated materials have a larger measurement range.

Next, the violin chart was used to calculate the average measurement range of T1 and T2 in **Figure 4**, as shown in **Figure 5**.

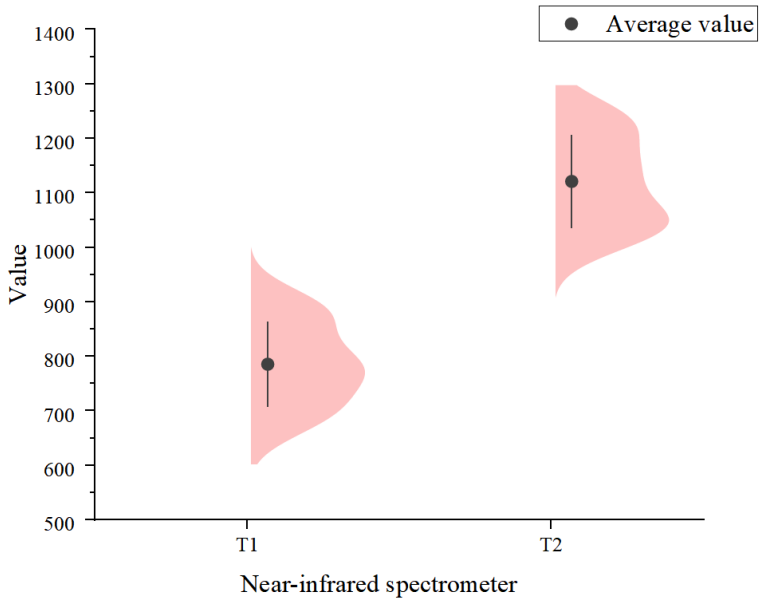

Figure 5. Average measurement range of T1 and T2.

The average measurement range of T1 calculated in **Figure 5** was 785.47 nanometers, while the average measurement range of T2 was 1121.13 nanometers. By dividing the mean difference between the measurement ranges of T1 and T2 by the average measurement range of T1, it can be concluded that the measurement range of T2 was 42.7% larger than that of T1.

4.3. Optical signal acquisition time

Five different frequencies were selected, namely 50.78 Hz, 58.59 Hz, 66.41 Hz, 74.22 Hz, and 82.03 Hz, to compare and analyze the T1 and T2 optical signal acquisition time under the influence of these five different frequencies. The acquisition frequency was set to 37 times. The collection time is shown in **Figures 6** and **7**.

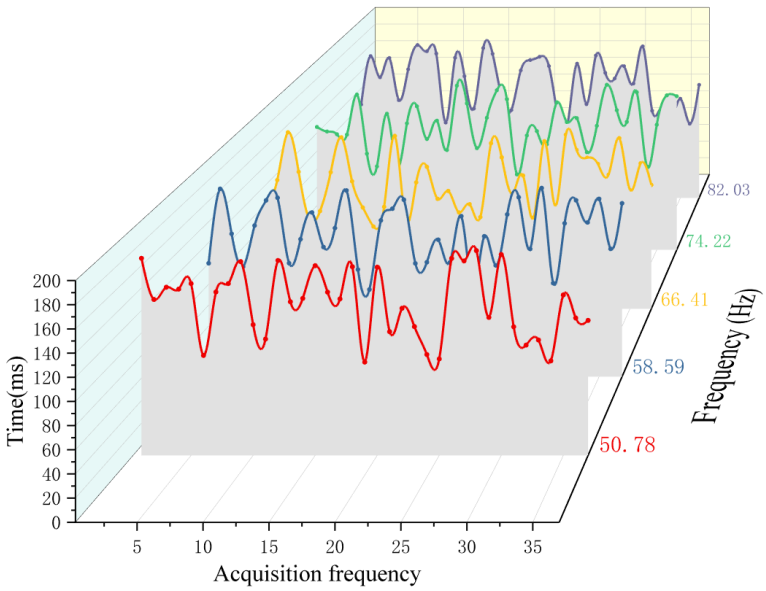

Figure 6. Optical signal acquisition time of T1 under different frequencies.

Figure 6 shows the optical signal acquisition time of T1 under the influence of five different frequencies. At a frequency of 50.78 Hz, the optical signal acquisition time range was distributed between 82.06 ms and 180.1 ms. When the frequency was 58.59 Hz, the collection time range of the optical signal was distributed between 82.65 ms and 179.3 ms. When the frequency was 66.41 Hz, the collection time range of the optical signal was distributed between 84.01 ms and 180.26 ms. When the frequency was 74.22 Hz, the collection time range of the optical signal was distributed between 82.3 ms and 180.16 ms. When the frequency was 82.03 Hz, the collection time range of the optical signal was distributed between 86.36 ms and 177.83 ms.

According to the data, it can be concluded that the optical signal acquisition time of T1 under the influence of 5 different frequencies exceeded 80 ms.

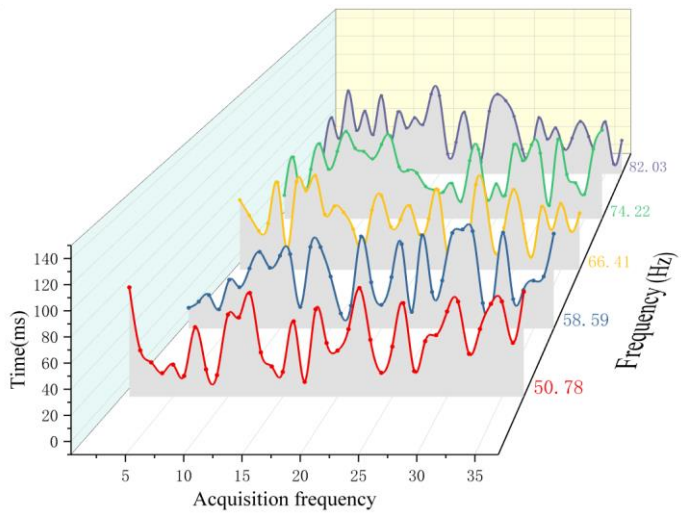

Figure 7. Optical signal acquisition time of T2 under different frequencies.

Figure 7 shows the optical signal acquisition time of T2 under the influence of five different frequencies. At a frequency of 50.78 Hz, the optical signal acquisition time range was distributed between 2.11 ms and 78.87 ms. When the frequency was 58.59 Hz, the collection time range of the optical signal was distributed between 3.3 ms and 77.09 ms. When the frequency was 66.41 Hz, the collection time range of the optical signal was distributed between 2.69 ms and 78.93 ms. When the frequency was 74.22 Hz, the collection time range of the optical signal was distributed between 3.54 ms and 79.59 ms. When the frequency was 82.03 Hz, the collection time range of the optical signal was distributed between 0.96 ms and 79.31 ms.

The data showed that the optical signal acquisition time of T2 under the influence of 5 different frequencies did not exceed 80 ms. The optical signal acquisition time of T2 was significantly shorter than that of T1. That is to say, T2 can complete the sampling and measurement of optical signals faster, which helps to better capture signals and signal details of rapid muscle changes, saving measurement time.

Independent sample T test was conducted for the acquisition time of optical signals T1 and T2 at each frequency, and the results were shown in **Table 8** below:

Table 8. T test of optical signal acquisition time.

Frequency	Mean variance	*T*-value	Degree of freedom	*P* value	Significance
50.78	90.59	21.07	72	< 0.001	Remarkable
58.59	90.78	21.16	72	< 0.001	Remarkable
66.41	91.33	21.28	72	< 0.001	Remarkable
74.22	89.66	20.89	72	< 0.001	Remarkable
82.03	91.96	21.51	72	< 0.001	Remarkable

Table 8 shows that T1 and T2 have significant differences in optical signal acquisition time at all frequencies (*P* value < 0.001), and T2's optical signal acquisition time is significantly shorter than T1's.

Based on the data results, the real-time monitoring system is designed by using the fast-sampling capability of T2 to help coaches and athletes get immediate physiological feedback and make scientific adjustments during training. At the same time, according to different sports and individual differences, combined with rapidly collected light signal data, customized training and rehabilitation programs to improve training efficiency and effect.

4.4. Measurement accuracy

The Results software accompanying the near infrared spectrometer was used to record the measurement accuracy of muscle oxygenation levels in T1 and T2 for 15 athletes, as shown in **Figure 8**.

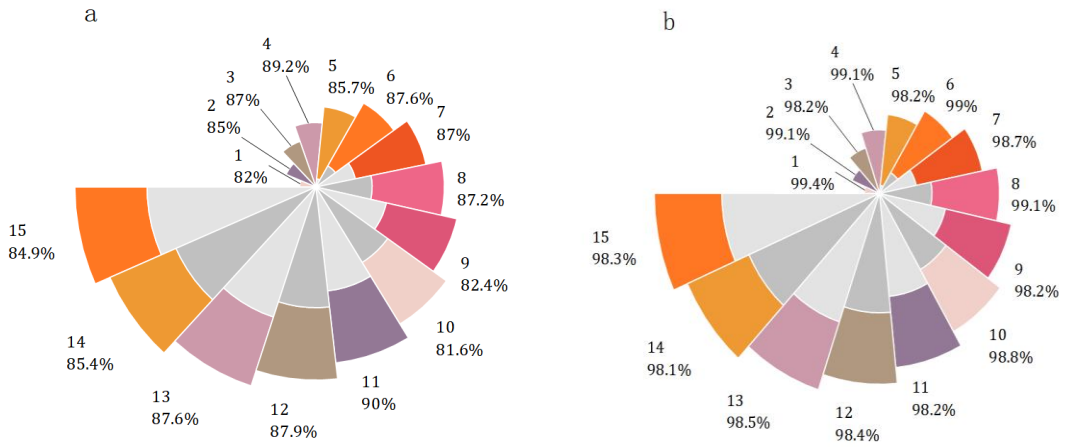

Figure 8. Measurement accuracy of T1 and T2: **(a)** Measurement accuracy of T1; **(b)** measurement accuracy of T2.

Figure 8 records the accuracy of T1 and T2 measurements of muscle oxygenation levels in 15 athletes. Among them, **Figure 8a** reflected that the measurement accuracy of T1 was between 81.6% and 90%. **Figure 8b** reflected the measurement accuracy of T2 between 98.1% and 99.4%.

Obviously, T2 had the highest measurement accuracy, both exceeding 98%. In summary, near infrared spectrometers using photosensitive π-conjugated materials had the best performance, which is conducive to real-time measurement of muscle oxygenation levels.

The above experimental data have well verified that the near infrared

spectrometer optimized using photosensitive π-conjugated materials in this paper has the best measurement performance.

5. Conclusions

Near infrared spectroscopy imaging analysis of NIR photosensitive π-conjugated materials has broad application prospects in sports science, especially in real-time measurement of muscle oxygenation levels. Photosensitive π-conjugated materials can achieve efficient absorption of near infrared light due to their strong photosensitivity and wide absorption spectrum range. On this basis, optimizing the design of the near infrared spectrometer using this material can effectively improve its sensitivity and signal-to-noise ratio, thereby improving its measurement performance. The near infrared spectrometer optimized using photosensitive π-conjugated materials in this article is superior to the near infrared spectrometer without photosensitive π-conjugated materials in terms of measurement range, light signal acquisition time, and measurement accuracy, with significant measurement results. Optimization of near infrared spectroscopy imaging analysis not only enables real-time monitoring of athletes' training effectiveness and rehabilitation progress, but also helps coaches develop more reasonable training plans and improve athletes' training effectiveness. With the continuous progress of technology, NIR imaging technology would play an increasingly important role in sports science.

Author contributions: Conceptualization, HH and NZ; methodology, HH; software, NZ; validation, HH and NZ; formal analysis, HH; investigation, NZ; resources, NZ; data curation, NZ; writing—original draft preparation, HH; writing—review and editing, NZ; visualization, NZ; supervision, HH; project administration, HH; funding acquisition, NZ. All authors have read and agreed to the published version of the manuscript.

Ethical approval: Not applicable.

Conflict of interest: The authors declare no conflict of interest.

References

1. Yan H, Bi X, Zheng X, et al. Breakpoints of SEMG and Muscle Oxygen in Incremental Exercise Test as well as the Evaluation of Anaerobic Threshold by Their Combination. Journal of Tianjin University of Sport. 2020; 35(6): 691–696.
2. Chen G, Jiang X, Dai J, Qin X. Study on the Change Characteristics of Muscle Oxygen Technology in the Increasing Load Exercise. Sport Science and Technology. 2020; 41(4): 35–38.
3. Xiong C, Wan Q, Xiao F, et al. Personalized Exercise Prescription Based on Muscle Oxygen Saturation Monitoring in Patients with Diabetes. Shanghai Nursing. 2020; 20(11): 11–14.
4. Yang L, Wei X, Li J. The influence of cardiac rehabilitation exercise guidance mode based on heart rate and muscle oxygen monitoring on the exercise tolerance of muscle oxygen saturation in patients with coronary atherosclerotic heart disease after percutaneous coronary intervention. Journal of Practical Medical Technology. 2021; 28(10): 1243–1246.
5. Jiang XY, Dai JS. Research Overview on Oxygenation Measuring Technique and Its Application in Sports. Journal of Nanjing Sports Institute. 2018; 1(12): 48–53.
6. Li Q, Hou G, Yuan S. Clinical study of neuromuscular electrical stimulation combined with muscle oxygen monitoring in the treatment of hemiplegia after stroke with lower extremity resistance training. Sichuan Journal of Physiological Sciences. 2023; 45(7): 1212–1215.

7. Duan N, Li R. Clinical study on the Treatment of Hemiplegia Patients after Stroke with Resistance Training under the Guidance of neuromuscular electrical Stimulation and Muscle Oxygen Monitoring. Clinical Research. 2022; 30(10): 178–181.
8. Xiao Z, Yang M, Zhu H, et al. Effect of 12-week Fatmax intensity exercise on body composition and muscle oxygen saturation of obese college students. Journal of Qinghai Normal University (Natural Science Edition). 2022; 38(1): 57–62.
9. Gao T, Zou C, Li J, et al. Study on the Response of Muscle Oxygen Content and Vascular Elasticity to Load Exercise. Life Science Instruments. 2021; 19(3): 38–42.
10. Chen DY, Zhang H, Zhang ZL, et al. Research on the Origin Traceability of Honeysuckle Based on Improved 1D-VD-CNN and Near-Infrared Spectral Data. Spectroscopy and Spectral Analysis. 2023; 43(5): 1471–1477.
11. Duan J, Mu J, Pan W, et al. Spectral characteristics of brain functional near-infrared spectroscopic imaging in depression patients with and without anxiety symptoms. Journal of Clinical Psychosomatic Diseases. 2023; 29(3): 18–22.
12. Zhang Z, Han N, Zhou T, et al. Identification of the Age of Aged Vinegar Based on Two-dimensional Correlation Near Infrared Spectroscopy. Journal of Chinese Institute of Food Science and Technology. 2023; 23(8): 389–395.
13. Chang J, Ma M, Sun D. Rapid Quality Evaluation of the Concentrated Liquid of Liuwei Dihuang Pills by Near-Infrared Spectroscopy. Hans Journal of Medicinal Chemistry. 2023; 11(1): 1–6.
14. Hu W, Tang W, Li C, et al. Estimating Nitrogen Concentration of Rubber Leaves Based on a Hybrid Learning Framework and Near-Infrared Spectroscopy. Spectroscopy and Spectral Analysis. 2023; 43(7): 2050–2058.
15. Zhu L, Lv Y, Du Q, et al. Construction and Application of Detection Model for Threonine and Valine Content in Buckwheat Leaves Based on Near Infrared Spectroscopy. Spectroscopy and Spectral Analysis. 2023; 43(S01): 5–6.
16. Liang L, Wu T, Shen K, et al. Prediction of Basic Density of Wood Chips Using Near-Infrared Spectroscopy and Moisture Content Correction Algorithm. Spectroscopy and Spectral Analysis. 2023; 43(8): 2476–2482.
17. Hao X, Peng Y, Yang Z, et al. Design of tobacco formulation based on the quality characterization by near infrared spectroscopy. Journal of Hunan Agricultural University: Natural Sciences. 2023; 49(3): 284–290.
18. Ge C, Zhao S, Zhang H, et al. Establishment and Verification of Near-infrared Spectral Prediction Model for Fat Content of Xanthoceras sorbifolia. Journal of Hebei Agricultural Sciences. 2023; 27(1): 104–108.
19. Zhao Y, Yin L, Shao X. Research on near-infrared spectroscopy discriminant model for rapid identification of drugs. Drug Standards of China. 2023; 24(4): 351–355.
20. Guo Y, Huang Y, Huang C, et al. Analysis of Blood Oxygen Content in Gingival Tissue of Patients with Periodontitis Based on Visible and Near-Infrared Spectroscopy. Spectroscopy and Spectral Analysis. 2023; 43(8): 2563–2567.
21. Liang J, Zhao X, Li L, et al. Model construction for nutrient content detection of Minqin lamb based on near-infrared spectroscopy. Food and Fermentation Industries. 2023; 49(14): 272–279.
22. Liang J. Research on the Application Effect of Near Infrared Spectroscopy in Short Track Speed Skaters' Aerobic Threshold Training. Bulletin of Sport Science & Technology. 2018; 26(3): 54–57.
23. Qu G, Chen Z, Zhang Q. Study on germination rate of rice seed based on uninformation variable elimination method. Jiangsu Journal of Agricultural Sciences. 2019; 35(5): 1015–1020.
24. Li L, Liu C, Zhao L. Estimation and Variable Selection of Logistic Regression Coefficient Based on Penalizing Maximum Lq Likelihood. Journal of Gansu Sciences. 2022; 34(3): 21–25.
25. Sun J, Zhang W, Shi J, Li Y. Selection and Application of Spectral Data Preprocessing Strategy. Acta Metrologica Sinica. 2023; 44(08): 1284–1292.
26. Yin X, Gu W. Near Infrared Spectrum Denoising Based on Lifting Wavelet Transform and Savitzky-Golay Filter. Chinese Journal of Sensors and Actuators. 2023; 36(3): 404–410.
27. Huang M, Li M, Dai Y. Based on the Savitzky-Golay Noise Reduction Algorithm of a Deep Foundation Pit Monitoring Data Processing. Journal of Shantou University: Natural Science Edition. 2022; 37(2): 50–60.
28. Shi J, Shen Y, Ma S, Shu C. Verifying Lambert-Beer law and measuring the solute concentration of multi-solute liquids using Phyphox software. Physics Experimentation. 2023; 43(4): 44–48.
29. Xin W. The applicable conditions and limitations of Lambert-Beer Law. Chemical Times. 2020; 34(7): 49–51.
30. Wang Y, Wang G, Liu R. Research on robustness of aviation manufacturing knowledge network based on variable standardization. Manufacturing Automation. 2020; 42(8): 63–67.
31. Jin Y, He W. Identification of Traditional Chinese Medicine Species Based on Multiple Scattering Correction. Electronic Production. 2022; 30(22): 90–92, 99.

32. Chen Y, Guo Y, Wang W, et al. Clustering Analysis of FTIR Spectra Using Fuzzy K-Harmonic-Kohonen Clustering Network. Spectroscopy and Spectral Analysis. 2023; 43(1): 268–272.
33. Zhou Y, Jiang S, Li Y, et al. Near-Infrared Hyperspectral Identification of Flue-Cured Tobacco Producing Areas. Journal of Changchun University of Science and Technology (Natural Science Edition). 2023; 46(4): 17–22.
34. Zhu X, Tuo X, Zhang G, et al. Comparison of FT-NIR Spectral Pretreatment and Characteristic Band Screening for Baijiu-based Liquor. Modern Food Science and Technology. 2023; 39(1): 196–204.
35. Xin P, Ji X, Shan T, Chen W. Evaluation of water resources carrying capacity in Jiangsu Province based on principal component analysis. Express Water Resources & Hydropower Information. 2023; 44(7): 27–32.
36. Jiang L, Zheng D. Analysis of the Factors of Employment of Computer Network Technology Majors in Vocational Colleges Based on the Principal Component Analysis under the Matlab Environment. Journal of Chongqing Electric Power College. 2023; 28(1): 68–74.